THE JOURNAL OF PHYSICAL CHEMISTRY A
A JOURNAL OF THE AMERICAN CHEMICAL SOCIETY

pubs.acs.org/JPCA Article

Double σ-Aromaticity in a Planar Zinc-Doped Gold Cluster: Au_9Zn^-

Published as part of The Journal of Physical Chemistry virtual special issue "Alexander Boldyrev Festschrift".

Maksim Kulichenko, Wei-Jia Chen, Yang-Yang Zhang, Cong-Qiao Xu,* Jun Li,* and Lai-Sheng Wang*

Cite This: *J. Phys. Chem. A* 2021, 125, 4606–4613 Read Online

ACCESS | Metrics & More | Article Recommendations | Supporting Information

ABSTRACT: The strong relativistic effects result in many interesting chemical and physical properties for gold and gold compounds. One of the most surprising findings has been that small gold clusters prefer planar structures. Dopants can be used to tune the electronic and structural properties of gold nanoclusters. Here we report an experimental and theoretical investigation of a Zn-doped gold cluster, Au_9Zn^-. Photoelectron spectroscopy reveals that Au_9Zn^- is a highly stable electronic system with an electron binding energy of 4.27 eV. Quantum chemical studies show that the global minimum of Au_9Zn^- has a D_{3h} structure with a closed-shell electron configuration ($^1A_1'$), which can be viewed as replacing the central Au atom by Zn in the open-shell parent Au_{10}^- cluster. The high electronic stability of Au_9Zn^- is corroborated by its extremely large HOMO–LUMO gap of 3.3 eV. Chemical bonding analyses revealed that the D_{3h} Au_9Zn^- are bonded by two sets of delocalized σ bonds, giving rise to double σ aromaticity and its remarkable stability. Two planar low-lying isomers are also observed, corresponding to a similar triangular structure with the Zn atom on the edge and another one with one of the corner Au atoms moved to the edge of the triangle.

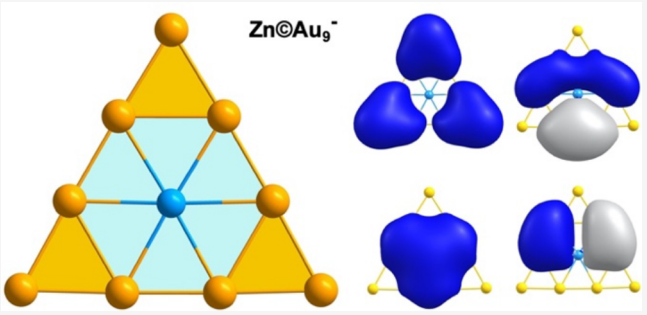

1. INTRODUCTION

Since it was first proposed to rationalize the apparent stability of cyclopropane,[1] the concept of σ-aromaticity has been used to explain the bonding in a wide variety of chemical systems.[2−28] It has been particularly valuable to understand the bonding and stability of the all-metal aromatic and antiaromatic systems[29−44] and boron clusters.[45−60] Gold clusters have received tremendous attention over the past 2 decades,[61−65] because of the discovery of catalytic effects by gold nanoparticles.[66,67] One of the most surprising findings is that negatively charged gold clusters (Au_n^-) can be planar up to Au_{12}^-.[68−70] The planarity has been generally understood to be due to the strong relativistic effects that can induce 6s−5d hybridization.[71−75] The Au_6^- cluster was in fact first proposed to be a D_{6h} ring based on the observation of a single vibrational progression in photodetachment spectroscopy.[76] A subsequent theoretical calculation found that the global minimum of Au_6^- was a triangle with D_{3h} symmetry,[77] which was confirmed by joint experimental and theoretical investigations.[68,78] Photoelectron spectroscopy of Au_6^- revealed that the neutral Au_6 cluster is an exceptionally stable electronic system with a large HOMO–LUMO gap.[76,79] The high stability of the Au_6 cluster with six valence electrons was confirmed by the isoelectronic Au_5Zn^+ cluster, which was found to exhibit σ-aromaticity.[80] σ-aromaticity was also found in the planar Au_6Y^- cluster with 10 valence electrons.[81] However, chemical bonding in the larger planar gold clusters has not been examined. An interesting question is the following: Is σ-aromaticity a general bonding feature for all the planar gold clusters?

The Au_{10}^- cluster is interesting and its global minimum also has a D_{3h} triangular structure.[68,78] Photoelectron spectroscopy (PES) of Au_{10}^- showed the presence of minor isomers with lower electron binding energies and the main isomer with a very high electron binding energy.[78] Theoretical calculations confirmed that the global minimum of Au_{10}^- is the D_{3h} structure with a high electron binding energy, while two other lowing-lying planar isomers with lower symmetries (D_{2h} and C_{2h}) have lower electron binding energies in agreement with the experimental observation. It was subsequently shown that the global minimum D_{3h} Au_{10}^- was inert toward O_2, but the lower symmetry D_{2h} and C_{2h} isomers were reactive with O_2 and could be titrated out of the cluster beam.[82] The high binding energy of the D_{3h} global minimum was due to the fact that neutral Au_{10} is open shell with two unpaired electrons occupying a doubly degenerate HOMO, similar to that of the Au_{16} cage cluster.[83] Thus, both Au_{10}^- and Au_{16}^- are doublets with one unpaired electron and unusually high electron

Received: April 1, 2021
Revised: May 7, 2021
Published: May 20, 2021

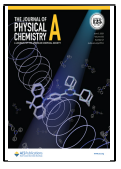

https://doi.org/10.1021/acs.jpca.1c02954
J. Phys. Chem. A 2021, 125, 4606–4613

binding energies, which explained their inertness toward O_2 whereas all other even sized Au_n^- clusters between $n = 2-20$ are highly reactive with O_2.[84] The open shell nature of the Au_{16}^- cluster was confirmed by doping a monovalent atom inside the Au_{16} cage, $M@Au_{16}^-$.[85]

For Au_{10}^- on the other hand, substitution of an Au atom by a divalent atom, such as Zn, should create a closed shell Au_9Zn^- with similar bonding properties as the parent if the D_{3h} symmetry can be maintained. Small Zn-doped clusters, Au_nZn^- ($n < 7$), have been studied experimentally and the Zn atom was shown not to change the planarity of the parent Au_{n+1}^- clusters in this size regime.[80,86−88] Cu and Ag atoms have been shown to simply substitute an Au atom of the Au_{10}^- parent in the Au_9Cu^- and Au_9Ag^- doped clusters,[89] whereas Y-doping has been shown to result in a 3D structure for Au_9Y.[90] A previous computational study showed that Au_9Zn^- maintained the triangular structure of Au_{10}^- with a closed-shell configuration and a lower C_s symmetry ($^1A'$).[91] The objective of the current work is to investigate the geometrical and electronic structure of Au_9Zn^- and assess if σ-aromaticity plays a role in its chemical bonding using a joint PES and relativistic quantum chemical study.

Well-resolved photoelectron spectra are obtained for Au_9Zn^- at two photon energies and are used to verify the obtained structures from the theoretical calculations. The electron affinity (EA) of Au_9Zn is measured to be extremely high (4.27 eV). In addition, minor isomers with lower electron binding energies are also observed. Global minimum structural searches reveal that the triangular closed-shell D_{3h} cluster with a central Zn atom is the most stable structure with two lower symmetry low-lying planar isomers. The calculated high binding energy and the simulated photoelectron spectrum of the closed-shell D_{3h} global minimum are in good agreement with the experimental data. The D_{3h} Au_9Zn^- is found to be an extremely stable electronic system with a large HOMO−LUMO gap. Chemical bonding analyses show that the D_{3h} Au_9Zn^- consists of two delocalized σ systems: three seven-center−two-electron (7c−2e) bonds describing the bonding between the Zn atom and its six nearest Au atoms; and three 3c−2e bonds at the three corners of the D_{3h} structure. Thus, the Au_9Zn^- cluster can be viewed to be doubly σ-aromatic.

2. METHODS

2.1. Photoelectron Spectroscopy. The experiment was conducted using a magnetic-bottle PES apparatus equipped with a laser-vaporization supersonic cluster source, details of which have been published elsewhere.[54,92] The Au_9Zn^- clusters were produced by laser vaporization of a disk target prepared by mixing powders of Au and Zn (Au/Zn molar ratio: 6/1). The laser-induced plasma was cooled by a high pressure He carrier gas seeded with 5% Ar, initiating nucleation and cluster formation. The nascent clusters were then entrained by the carrier gas and underwent a supersonic expansion to produce a cold cluster beam. After passing a skimmer, negatively charged clusters were extracted perpendicularly from the collimated cluster beam and analyzed using time-of-flight mass spectrometry. The Au_9Zn^- clusters of interest were mass-selected and decelerated before photodetachment. Two photon energies were used in the current experiment: 266 nm (4.661 eV) from a Nd:YAG laser and 193 nm (6.424 eV) from an ArF excimer laser. Photoelectrons were collected at nearly 100% efficiency by the magnetic bottle and analyzed in a 3.5 m long electron flight tube. The photoelectron kinetic energy (E_k) was calibrated using the known spectrum of Bi^-. The resolution of the magnetic-bottle photoelectron analyzer was $\Delta E_k/E_k \approx 2.5\%$, that is, around 25 meV for electrons with 1 eV kinetic energy.

2.2. Computational Details. The theoretical studies were carried out using both density functional theory (DFT) and wave function theory (WFT) methods. Global minimum searches were performed using the AFFCK code,[93] and geometry optimizations were done at the PBE0/LANL2DZ level of theory[94] as implemented in Gaussian-16.[95] The AFFCK code is an efficient global optimization method through the introduction of an intermediate step where structures are optimized using a classical force field generated on the fly within the algorithm.[93] About 7000 initial structures were generated and optimized at the PBE0 level of theory. Both singlet and triplet spin states were tested for each generated structure. Then, the lowest energy isomers were reoptimized at higher levels of DFT and WFT, i.e., PBE0/def2-TZVP, PBE0/aug-cc-pVTZ, and CCSD(T)/def2-TZVP//PBE0/def2-TZVP. Additionally, the relative order of isomers was tested using scalar relativistic corrections at the PBE0/ZORA-def2-TZVP level as implemented in the ORCA package.[96] Corrections for the relativistic effects did not change the relative order of the isomers. Only structures with the singlet spin state were present in low-lying isomers. The closed-shell singlet character of the global minimum was supported by the wave function stability test (stable = opt) and the determinant coefficients in CASSCF(8,8)/def2-TZVP calculations. We also conducted global minimum searches using the TGMin code[97] and obtained similar low-lying isomers as the AFFCK searches. The TGMin code is based on a constrained basin-hopping algorithm and the generation of structures is based on point group symmetries and random perturbations. Both planar and three-dimensional (3D) isomers were considered via a comprehensive study of structures with various point group symmetries.

Electronic structure, Kohn−Sham molecular orbital (MO) energy-level correlation diagram, the vertical detachment energies (VDE) and spectral simulations were performed using the DFT method as implemented in ADF 2016.106.[98,99] The generalized gradient approximation (GGA) with the hybrid PBE0 exchange-correlation functional were used, together with the TZ2P Slater basis sets. Frozen core approximations were applied to the inner shells [$1s^2$ $2p^6$] for the Zn atom and [$1s^2$ $4d^{10}$] for the Au atoms. The scalar relativistic (SR) and spin−orbit (SO) coupling effects were taken into account using the zero-order-regular approximation (ZORA).[100] The first vertical detachment energy (VDE_1) was calculated as the energy difference between the neutral and anionic ground state at the optimized anion geometry. Higher binding energy detachment channels and the spectral simulations were calculated by considering the SO effects via the generalized Koopmans theorem (GKT), which could qualitatively account for the trend and ordering of VDEs as reported previously.[101−104] Chemical bonding was analyzed using the adaptive natural density partitioning (AdNDP) approach developed by Zubarev and Boldyrev,[105−107] at the PBE0/LANL2DZ level of theory as implemented in Gaussian-16.

3. RESULTS

3.1. Experimental Results. The photoelectron spectra of Au_9Zn^- at 266 and 193 nm are shown in Figure 1. The 266 nm

https://doi.org/10.1021/acs.jpca.1c02954
J. Phys. Chem. A 2021, 125, 4606−4613

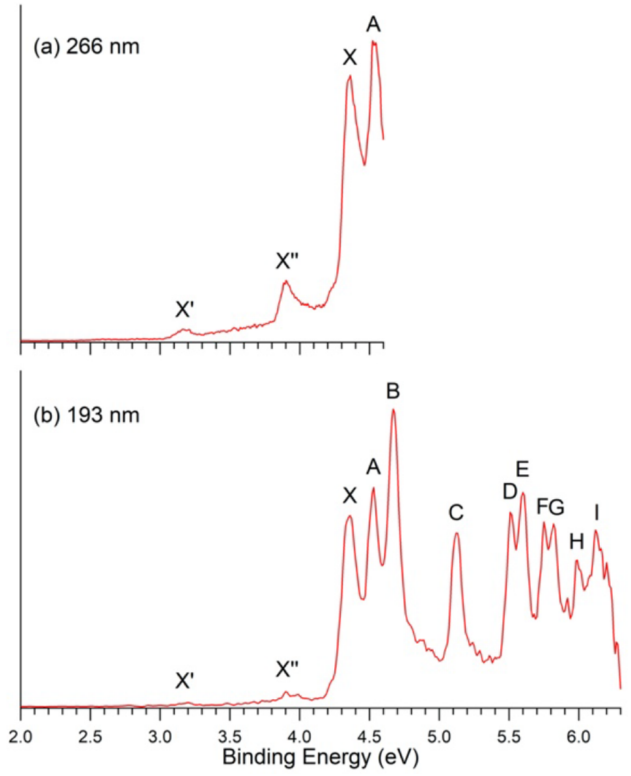

Figure 1. Photoelectron spectroscopy of Au_9Zn^- at (a) 266 nm (4.661 eV) and (b) 193 nm (6.424 eV).

spectrum (Figure 1a) displays two well-resolved PES bands X and A with VDEs at 4.36 and 4.53 eV, respectively. The adiabatic detachment energy (ADE) of band X is estimated from its onset to be 4.27 eV, which represents the EA of the corresponding neutral Au_9Zn. Eight more well-resolved PES bands are observed in the 193 nm spectrum (Figure 1b), labeled from B to I. The VDEs of all the observed PES bands are given in Table S1, where they are compared with the theoretical results to be discussed below. Two weak bands X′ and X″ are also observed on the lower binding energy side at 3.17 and 3.90 eV, respectively. The relative intensities of these features are reduced in the 193 nm spectrum, suggesting that they are likely due to contributions from low-lying isomers of Au_9Zn^-.

3.2. Theoretical Results. The structures found within 20 kcal/mol of the global minimum are shown in Figure S1. The first three low-lying isomers are all closed-shell planar structures, as displayed in Figure 2. The lowest energy structure of Au_9Zn^- was found to be planar with D_{3h} symmetry at different levels of theory. It is a triangular structure with the Zn atom at the center; its detailed bond lengths are depicted in Figure S2. The second low-lying isomer (Iso1) is similar to the global minimum with the Zn atom on the edge of the triangle; it is 10.7 kcal/mol higher in energy than the D_{3h} structure at the CCSD(T) level. The third isomer (Iso2) can be described as moving one of the apex Au atoms of the D_{3h} structure to the opposite edge. Iso1 and Iso2 are basically positional isomers of the D_{3h} global minimum with the displacement of one atom.

Because of the stability of the planar structures, there are large energy barriers between the different isomers despite the apparent similarity of these structures. We searched for the transformation between Iso2 and the global minimum, as shown in Figure S3, where a barrier of 20.1 kcal/mol was found from Iso2 to the D_{3h} structure. As will be shown below, the large energy barriers are important to understand the observation of Iso1 and Iso2 in our experiment despite their relatively high energies above the global minimum.

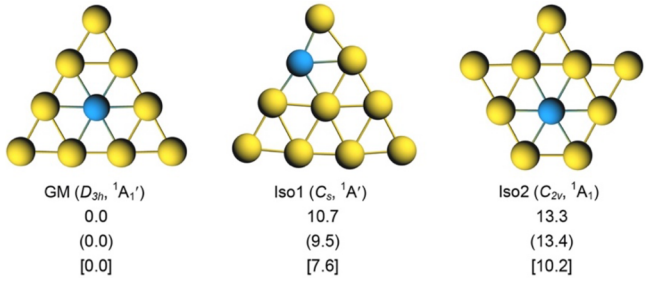

Figure 2. Global minimum (GM) and low-lying isomers of Au_9Zn^- and their relative energies. All energies are in kcal/mol at the CCSD(T)/def2-TZVP//PBE0/def2-TZVP, PBE0/def2-TZVP (in parentheses), and PBE0/TZ2P (in brackets) levels.

4. DISCUSSION

4.1. Confirmation of the Global Minimum of Au_9Zn^-. To confirm the global minimum of Au_9Zn^-, we have calculated the first VDE (VDE_1) for the top three lowest energy isomers, as compared with the experimental data in Table 1. The VDE_1 computed for the D_{3h} global minimum, 4.42 eV at the PBE0 level or 4.28 eV at the CCSD(T) level, is in excellent agreement with the VDE of the X band at 4.36 eV. The theoretical values for the VDE_1 of Iso1 and Iso2 are in good agreement with those measured for the weak peaks X′ and X″, respectively.

We also computed the higher VDEs of the D_{3h} structure using the GKT approach, as compared with the experimental data in Table S1. The higher VDEs were computed by adding the first VDE from the CCSD(T)/def2-TZVP calculations to the excitation energies computed for the neutral Au_9Zn. A simulated spectrum was obtained by fitting the VDEs with unit area Gaussian functions of 0.02 eV width,[42] as compared with the 193 nm spectrum in Figure 3. The simulated spectrum almost perfectly reproduces the experimental spectral features.

The first PES band X represents the transition from the ground state of the D_{3h} Au_9Zn^- to that of the corresponding neutral compound, due to electron detachment from the HOMO (34e′, Figures 4 and 5). Because of the strong spin−orbit coupling, removal of an electron from the doubly degenerate 34e′ orbitals results in two detachment channels corresponding to peaks X and A, as shown in Table S1. The calculated VDEs of 4.28 and 4.41 eV are in good agreement with the experimental VDEs for peaks X (4.36 eV) and A (4.53 eV), respectively. The next detachment channel is from the $20a_1'$ orbital with a calculated VDE of 4.67 eV, in excellent agreement with the VDE of peak B (4.67 eV). The 34e′ and $20a_1'$ orbitals are mainly composed of the Au 6s atomic orbitals (AOs), as shown in the energy-level correlation diagram (Figure 4) and the MOs in Figure 5. Following an energy gap, higher detachment channels are mainly derived from the Au 5d-dominated orbitals or 6s−5d hybrid orbitals (Figure 4 and Figure S4). All the calculated VDEs are in good agreement with the observed features (Table S1). The overall excellent agreement between the simulated and the observed spectrum, as shown in Figure 3, provides unequivocal evidence for the D_{3h} structure as the global minimum of Au_9Zn^-.

https://doi.org/10.1021/acs.jpca.1c02954
J. Phys. Chem. A 2021, 125, 4606−4613

Table 1. Comparison of the Experimental and Calculated VDE_1 for the Global Minimum D_{3h} Structure and the Two Low-Lying Isomers, Iso1 and Iso2, of Au_9Zn^- at Two Levels of Theory

			VDE_1(theor)	
isomer	electron configuration	VDE_1(exp)	PBE0/def2-TZVP	CCSD(T)/def2-TZVP
D_{3h}	$...(a_1')^2(e')^3(e')^0$	4.36	4.42	4.28
Iso1, C_s	$...(a')^2(a')^1(a')^0$	3.90	3.77	3.83
Iso2, C_{2v}	$...(a)^2(a)^1(a)^0$	3.17	3.38	3.37

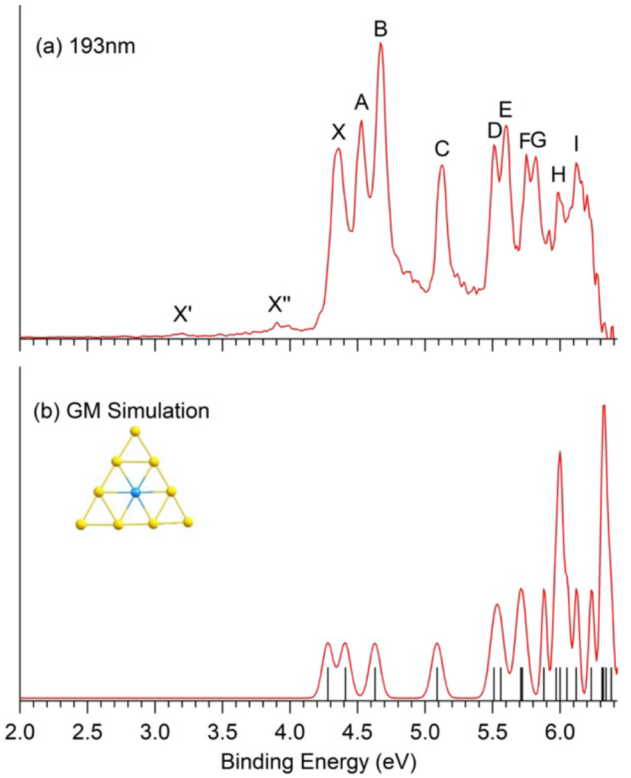

Figure 3. Comparison of the simulated spectrum for the global minimum of D_{3h} Au_9Zn^- with the experimental spectrum at 193 nm. The simulated spectrum is obtained via the GKT approach at the PBE0/TZ2P SO-ZORA level.

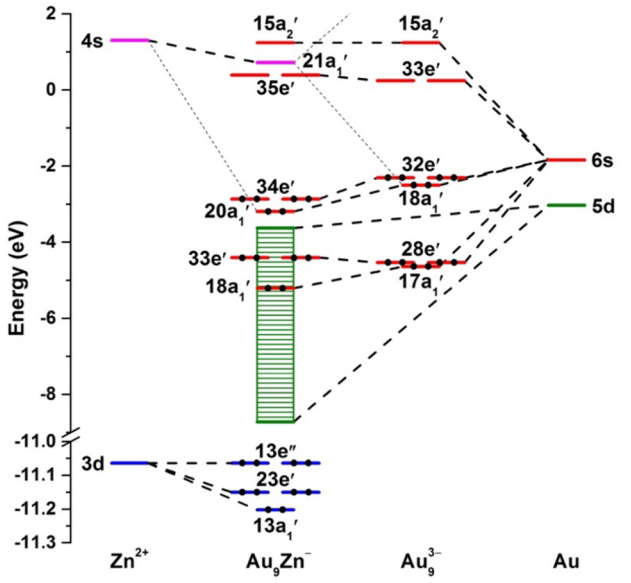

Figure 4. Kohn−Sham MO correlation diagram between Zn^{2+} and Au_9^{3-} for D_{3h} Au_9Zn^- at the PBE0/TZ2P SR-ZORA level via the ADF program. The energy levels in magenta, blue, red, and green denotes to the MOs derived from 4s(Zn), 3d(Zn), 6s(Au), and 5d(Au) AOs, respectively. Electrons on the occupied MOs are represented by dots.

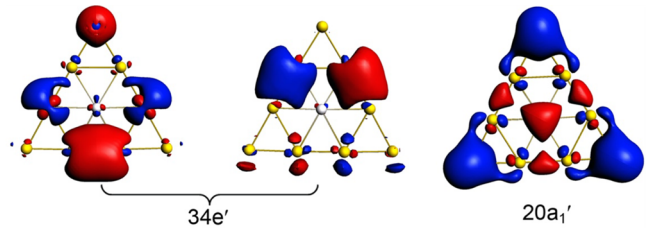

Figure 5. Contour plots of the 6s-based HOMO (34e′) and HOMO−1 ($20a_1'$) of the D_{3h} Au_9Zn^- at the PBE0/TZ2P SR-ZORA level via the ADF program.

The good agreement between the computed VDE_1 of the higher energy isomers, Iso1 and Iso2, and the weak peaks X′ and X″ (Table 1) suggests that they were present experimentally. However, Iso1 and Iso2 are 10.7 and 13.3 kcal/mol higher in energy than the global minimum, respectively, at the CCSD(T)/def2-TZVP level (Figure 1). These isomers were likely kinetically trapped once they were formed during the cluster growth because the large energy barriers separating them from the global minimum (Figure S3).

4.2. Chemical Bonding in the D_{3h} Au_9Zn^-. The global minimum D_{3h} Au_9Zn^- consists of a central Zn atom, three apex or corner Au atoms (Au_a) and six Au atoms at the edge sites (Au_e). The large electron binding energy of Au_9Zn^- (ADE, 4.27 eV; VDE, 4.36 eV) indicates that it is an extremely stable electronic system. The high electronic stability of D_{3h} Au_9Zn^- is borne out from the MO analysis shown in Figure 4, which indicates a large HOMO−LUMO energy gap of 3.3 eV at the PBE/def2-TZVP level. The D_{3h} structure of Au_9Zn^- is essentially the same as the parent D_{3h} Au_{10}^-, which is an open-shell system with an unpaired electron.[82] Substitution of the central Au atom by Zn in the D_{3h} Au_{10}^- cluster resulted in the stable closed-shell D_{3h} Au_9Zn^- with 12 valence electrons, a magic number in the 2D jellium model.[87]

As can be seen from Figure 5, the pattern of the 34e′ and $20a_1'$ orbitals are reminiscent of a typical σ-aromatic system with $4n + 2$ ($n = 1$) electrons, as discussed for the triangular Au_6 cluster[108] and several isoelectronic doped Au_6 clusters.[80,81,87] As indicated in Figure 4, significant 6s−5d hybridization occurs, primarily involving the 28e′ and $17a_1'$ orbitals on the Au_9^{3-} framework. To understand the structure and chemical bonding of Au_9Zn^- in more detail, we performed AdNDP analyses. Because of the d^{10}-configuration of Zn and Au, we have 100 out of 112 valence electrons localized as lone pairs with occupation numbers (ONs) of 1.99 lel. Out of the remaining 12 electrons, the AdNDP results revealed three 3c−

https://doi.org/10.1021/acs.jpca.1c02954
J. Phys. Chem. A 2021, 125, 4606−4613

2e σ bonds formed at the apex sites by one Au_a atoms and two adjacent Au_e atoms, as shown in Figure 6. The other three 7c−

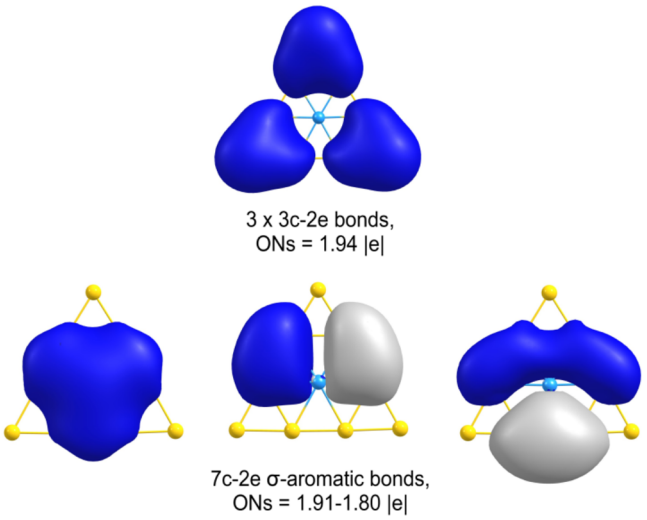

Figure 6. AdNDP bonding patterns of D_{3h} Au_9Zn^-. ON is the occupation number.

2e σ bonds describe the bonding of Zn with the six Au atoms in its first coordination shell. In fact, these three delocalized σ bonds are reminiscent of those in Au_6.[108]

Inasmuch as the localization of canonical MOs are not unique, we found that the three 7c−2e bonds can also be further represented by three 3c−2e bonds, as shown in Figure S5. However, the ONs of the three 3c−2e bonds are much lower (1.75 |el), which suggests that the 7c−2e representation better describes the bonding situation in Au_9Zn^-. The three 7c−2e bonds also display more vividly the σ aromaticity. Thus, the D_{3h} Au_9Zn^- cluster can be viewed to possess two σ aromatic systems, one describing the bonding between Zn and the its six nearest neighbors and a second σ system describing the bonding of the three corner Au atoms with the central $Zn@Au_6$ unit. The double σ aromaticity underlies the extremely high stability of the D_{3h} Au_9Zn^- cluster. The parent D_{3h} Au_{10} cluster with two unpaired electrons[82] should be considered a doubly σ Baird aromatic system for triplet staes.[44,109] The deviation of the ONs from 2 is an indication of the s−d hybridization. The larger ONs of the three 3c−2e bonds suggests they are primarily from the three 6s-based MOs shown in Figure 5. The larger deviation of the 7c−2e bonds from 2 indicates they are from MOs of significant s−d hybridization. The strong s−d hybridization, due to the relativistic effects of gold, is a major reason for the planarity of small gold clusters.[71−75]

5. CONCLUSIONS

We report a photoelectron spectroscopy and theoretical study of the Au_9Zn^- cluster. The photoelectron spectra revealed well-resolved spectral features, as well as evidence of two low-lying isomers. The global minimum of Au_9Zn^- was found to have a planar D_{3h} structure with a central Zn atom. Two planar low-lying isomers were found due to the displacements of one atom from the D_{3h} global minimum. The electron affinity of the D_{3h} Au_9Zn cluster was measured to be 4.27 eV, which is extremely high and indicates Au_9Zn^- is a very stable electronic system. The high electronic stability of the D_{3h} Au_9Zn^- is consistent with its large HOMO−LUMO gap of 3.3 eV computed at the PBE0 level. Chemical bonding analyses showed that the D_{3h} Au_9Zn^- cluster possesses two delocalized σ systems, one consisting of three 3c−2e bonds at the three corners and another consisting of Zn and its first coordination shell. The double σ-aromaticity further underlies the high stability of the D_{3h} Au_9Zn^-.

■ ASSOCIATED CONTENT

Supporting Information

The Supporting Information is available free of charge at https://pubs.acs.org/doi/10.1021/acs.jpca.1c02954.

Low-lying isomers of Au_9Zn^-, detailed structural parameter of the D_{3h} global minimum, energy profile for the transformation from Iso2 to the global minimum, selected valence MOs for the D_{3h} global minimum, an alternative AdNDP bonding pattern, and the experimental VDEs for the main isomer of Au_9Zn^-, compared with the computed values for the D_{3h} global minimum (PDF)

■ AUTHOR INFORMATION

Corresponding Authors

Cong-Qiao Xu − *Department of Chemistry, Southern University of Science and Technology, 518055 Shenzhen, China;* orcid.org/0000-0003-4593-3288; Email: xucq@sustech.edu.cn

Jun Li − *Department of Chemistry and Key Laboratory of Organic Optoelectronics & Molecular Engineering of Ministry of Education, Tsinghua University, 100084 Beijing, China; Department of Chemistry, Southern University of Science and Technology, 518055 Shenzhen, China;* orcid.org/0000-0002-8456-3980; Email: junli@tsinghua.edu.cn

Lai-Sheng Wang − *Department of Chemistry, Brown University, Providence, Rhode Island 02912, United States;* orcid.org/0000-0003-1816-5738; Email: lai-sheng_wang@brown.edu

Authors

Maksim Kulichenko − *Department of Chemistry and Biochemistry, Utah State University, Logan, Utah 84322, United States*

Wei-Jia Chen − *Department of Chemistry, Brown University, Providence, Rhode Island 02912, United States*

Yang-Yang Zhang − *Department of Chemistry and Key Laboratory of Organic Optoelectronics & Molecular Engineering of Ministry of Education, Tsinghua University, 100084 Beijing, China*

Complete contact information is available at: https://pubs.acs.org/10.1021/acs.jpca.1c02954

Notes

The authors declare no competing financial interest.

■ ACKNOWLEDGMENTS

The experiment done at Brown University was supported by the National Science Foundation (CHE-2053541). C.-Q.X. and J. L. are supported by the National Natural Science Foundation of China (Grant 22033005 and 22038002) and partially sponsored by the Guangdong Provincial Key Laboratory of Catalysis (No. 2020B121201002). Computational resources are supported by the Center for Computa-

tional Science and Engineering (SUSTech) and Tsinghua National Laboratory for Information Science and Technology. The support and resources from the Center for High Performance Computing at the University of Utah are gratefully acknowledged.

REFERENCES

(1) Dewar, M. J. S. Sigma-Conjugation and Sigma-Aromaticity. *Bull. Soc. Chim. Belg.* **1979**, *88*, 957−967.
(2) Schleyer, P. v. R.; Jiao, H.; Glukhovtsev, M. N.; Chandrasekhar, J.; Kraka, E. Double Aromaticity in the 3,5-Dehydrophenyl Cation and in Cyclo[6] carbon. *J. Am. Chem. Soc.* **1994**, *116*, 10129−10134.
(3) Jiao, H.; Schleyer, P. v. R.; Glukhovtsev, M. N. Are the D_{mh} Symmetric H_x^q Rings with $4n + 2$ 2-Electrons and Hydrogen Clusters Aromatic? *J. Phys. Chem.* **1996**, *100*, 12299−12304.
(4) Kuznetsov, A. E.; Boldyrev, A. I.; Zhai, H. J.; Li, X.; Wang, L.-S. Al_6^{2-} Fusion of Two Aromatic Al_3^- Units. A Combined Photoelectron Spectroscopy and *Ab Initio* Study of $M^+[Al_6^{2-}]$ (M = Li, Na, K, Cu, and Au). *J. Am. Chem. Soc.* **2002**, *124*, 11791−11801.
(5) Alexandrova, A. N.; Boldyrev, A. I. -Aromaticity and –Antiaromaticity in Alkali Metal and Alkaline Earth Metal Small Clusters. *J. Phys. Chem. A* **2003**, *107*, 554−560.
(6) King, R. B. Metal Cluster Topology. 21. Sigma Aromaticity in Triangular Metal Carbonyl Clusters. *Inorg. Chim. Acta* **2003**, *350*, 126−130.
(7) Li, Z. H.; Moran, D.; Fan, K. N.; Schleyer, P. v. R. K-Aromaticity and –Antiaromaticity in Saturated Inorganic Rings. *J. Phys. Chem. A* **2005**, *109*, 3711−3716.
(8) Havenith, R. W. A.; De Proft, F.; Fowler, P. W.; Geerlings, P. -Aromaticity in H_3^+ and Li_3^+: Insights from Ring-Current Maps. *Chem. Phys. Lett.* **2005**, *407*, 391−396.
(9) Fowler, P. W.; Rogowska, A.; Soncini, A.; Lillington, M.; Olson, L. P. Ring Currents in Tangentially p-p Bonded -Aromatic Systems. *J. Org. Chem.* **2006**, *71*, 6459−6467.
(10) Lin, Y. C.; Sundholm, D.; Juselius, J.; Cui, L. F.; Li, X.; Zhai, H. J.; Wang, L. S. Experimental and Computational Studies of Alkali-Metal Coinage-Metal Clusters. *J. Phys. Chem. A* **2006**, *110*, 4244−4250.
(11) Heine, T.; Islas, R.; Merino, G. α and Contributions to the Induced Magnetic Field: Indicators for the Mobility of Electrons in Molecules. *J. Comput. Chem.* **2007**, *28*, 302−309.
(12) Corminboeuf, C.; Schleyer, P. v. R.; King, R. B. Aromaticity of Tri- and Tetranuclear Metal-Carbonyl Clusters Based on Magnetic Criteria. *Chem. - Eur. J.* **2007**, *13*, 978−984.
(13) Höltzl, T.; Janssens, E.; Veldeman, N.; Veszpremi, T.; Lievens, P.; Nguyen, M. T. The Cu_7Sc Cluster is a Stable S-Aromatic Seven-Membered Ring. *ChemPhysChem* **2008**, *9*, 833−838.
(14) Jimenez-Halla, J. O. C.; Matito, E.; Blancafort, L.; Robles, J.; Sola, M. Tuning Aromaticity in Trigonal Alkaline Earth Metal Clusters and Their Alkali Metal Salts. *J. Comput. Chem.* **2009**, *30*, 2764−2776.
(15) Hatanaka, M.; Saito, M.; Fujita, M.; Morokuma, K. σ-Aromaticity in Hexa-Group 16 Atom-Substituted Benzene Dications: A Theoretical Study. *J. Org. Chem.* **2014**, *79*, 2640−2646.
(16) Cui, P.; Hu, H. S.; Zhao, B.; Miller, J. T.; Cheng, P.; Li, J. A Multicentre-Bonded $[Zn^I]_8$ Cluster with Cubic Aromaticity. *Nat. Commun.* **2015**, *6*, 6331.
(17) Zhu, C.; Zhou, X.; Xing, H.; An, K.; Zhu, J.; Xia, H. X-Aromaticity in an Unsaturated Ring: Osmapentalene Derivatives Containing a Metallacyclopropene Unit. *Angew. Chem., Int. Ed.* **2015**, *54*, 3102−3106.
(18) Freitag, K.; Gemel, C.; Jerabek, P.; Oppel, I. M.; Seidel, R. W.; Frenking, G.; Banh, H.; Dilchert, K.; Fischer, R. A. The F-Aromatic Clusters $[Zn_3]^+$ and $[Zn_2Cu]$: Embryonic Brass. *Angew. Chem., Int. Ed.* **2015**, *54*, 4370−4374.
(19) Ivanov, A. S.; Zhang, X.; Wang, H.; Boldyrev, A. I.; Gantefoer, G.; Bowen, K. H.; Černušák, I. Anion Photoelectron Spectroscopy and CASSCF/CASPT2/RASSI Study of La_n^- (n = 1, 3−7). *J. Phys. Chem. A* **2015**, *119*, 11293−11303.
(20) Li, W. L.; Xu, C. Q.; Hu, S. X.; Li, J. Theoretical Studies on the Bonding and Electron Structures of a $[Au_3Sb_6]^{3-}$ Complex and Its Oligomers. *Dalton Trans.* **2016**, *45*, 11657−11667.
(21) Pan, F. X.; Xu, C. Q.; Li, L. J.; Min, X.; Wang, J. Q.; Li, J.; Zhai, H. J.; Sun, Z. M. A Niobium-Necked Cluster $[As_3Nb(As_3Sn_3)]^{3-}$ with Aromatic Sn_3^{2-}. *Dalton Trans.* **2016**, *45*, 3874−3879.
(22) Popov, I. A.; Pan, F. X.; You, X. R.; Li, L. J.; Matito, E.; Liu, C.; Zhai, H. J.; Sun, Z. M.; Boldyrev, A. I. Peculiar All-Metal -Aromaticity of the $[Au_2Sb_{16}]^{4-}$ Anion in the Solid State. *Angew. Chem., Int. Ed.* **2016**, *55*, 15344−15346.
(23) Popov, I. A.; Starikova, A. A.; Steglenko, D. V.; Boldyrev, A. I. Usefulness of the P-Aromaticity and –Antiaromaticity Concepts for Clusters and Solid-State Compounds. *Chem. - Eur. J.* **2018**, *24*, 292−305.
(24) Liu, C.; Popov, I. A.; Chen, Z.; Boldyrev, A. I.; Sun, Z. M. Aromaticity and Antiaromaticity in Zintl Clusters. *Chem. - Eur. J.* **2018**, *24*, 14583−14597.
(25) Tkachenko, N. V.; Boldyrev, A. I. Multiple Local p-Aromaticity of Nonagermanide Clusters. *Chem. Sci.* **2019**, *10*, 5761−5765.
(26) Dai, C.; Huang, Y.; Zhu, J. Adaptive σ Aromaticity and Triplet Ground State in Tetraatomic Boron Species. *Organometallics* **2020**, *39*, 2602−2608.
(27) Xu, H. L.; Popov, I. A.; Tkachenko, N. V.; Wang, Z. C.; Munoz-Castro, A.; Boldyrev, A. I.; Sun, Z. M. a-Aromaticity-Induced Stabilization of Heterometallic Supertetrahedral Clusters $[Zn_6Ge_{16}]^{4-}$ and $[Cd_6Ge_{16}]^{4-}$. *Angew. Chem., Int. Ed.* **2020**, *59*, 17286−17290.
(28) Kulichenko, M.; Boldyrev, A. I. σ-Aromaticity in the MoS_2 Monolayer. *J. Phys. Chem. C* **2020**, *124*, 6267−6273.
(29) Li, X.; Kuznetsov, A. E.; Zhang, H. F.; Boldyrev, A. I.; Wang, L. S. Observation of All-Metal Aromatic Molecules. *Science* **2001**, *291*, 859−861.
(30) Kuznetsov, A. E.; Birch, K. A.; Boldyrev, A. I.; Li, X.; Zhai, H. J.; Wang, L. S. All-Metal Antiaromatic Molecule: Rectangular Al_4^{4-} in the $Li_3Al_4^-$ Anion. *Science* **2003**, *300*, 622−625.
(31) Zhan, C. G.; Zheng, F.; Dixon, D. A. Electron Affinities of Al_n Clusters and Multiple-Fold Aromaticity of the Square Al_4^{2-} Structure. *J. Am. Chem. Soc.* **2002**, *124*, 14795−14803.
(32) Havenith, R. W. A.; van Lenthe, J. H. A Valence Bond Study of the *s* and *p* Aromatic Species Al_4^{2-}. *Chem. Phys. Lett.* **2004**, *385*, 198−201.
(33) Mercero, J. M.; Ugalde, J. M. Sandwich-Like Complexes Based on "All-Metal" (Al_4^{2-}) Aromatic Compounds. *J. Am. Chem. Soc.* **2004**, *126*, 3380−3381.
(34) Boldyrev, A. I.; Wang, L.-S. All-Metal Aromaticity and Antiaromaticity. *Chem. Rev.* **2005**, *105*, 3716−3757.
(35) Tsipis, C. A. DFT Study of "All-Metal" Aromatic Compounds. *Coord. Chem. Rev.* **2005**, *249*, 2740−2762.
(36) Lin, Y. C.; Jusélius, J.; Sundholm, D.; Gauss, J. Magnetically Induced Current Densities in Al_4^{2-} and Al_4^{4-} Species Studied at the Coupled-Cluster Level. *J. Chem. Phys.* **2005**, *122*, 214308.
(37) Nigam, S.; Majumder, C.; Kulshreshtha, S. K. Structure and Bonding of Tetramer Clusters: Theoretical Understanding of the Aromaticity. *J. Mol. Struct.: THEOCHEM* **2005**, *755*, 187−194.
(38) Havenith, R. W. A.; Fowler, P. W. The Origin of the Ring Current in the All-Metal Aromatic, Al_4^{2-}. *Phys. Chem. Chem. Phys.* **2006**, *8*, 3383−3386.
(39) Islas, R.; Heine, T.; Merino, G. Structure and Electron Delocalization in Al_4^{2-} and Al_4^{4-}. *J. Chem. Theory Comput.* **2007**, *3*, 775−781.
(40) Yang, L. M.; Ding, Y. H.; Sun, C. C. Sandwich-like Compounds Based on the All-Metal Aromatic Unit Al_4^{2-} and the Main-Group Metals M (M = Li, Na, K, Be, Mg, Ca). *Chem. - Eur. J.* **2007**, *13*, 2546−2555.
(41) Zubarev, D. Y.; Averkiev, B. B.; Zhai, H. J.; Wang, L. S.; Boldyrev, A. I. Aromaticity and Antiaromaticity in Transition-Metal Systems. *Phys. Chem. Chem. Phys.* **2008**, *10*, 257−267.

https://doi.org/10.1021/acs.jpca.1c02954
J. Phys. Chem. A 2021, 125, 4606−4613

(42) Feixas, F.; Matito, E.; Duran, M.; Poater, J.; Sola, M. Aromaticity and Electronic Delocalization in All-Metal Clusters with Single, Double, and Triple Aromatic Character. *Theor. Chem. Acc.* **2011**, *128*, 419−431.
(43) Feixas, F.; Matito, E.; Poater, J.; Sola, M. Metalloaromaticity. *WIREs Comput. Mol. Sci.* **2013**, *3*, 105−122.
(44) Chen, D.; Szczepanik, D. W.; Zhu, J.; Sola, M. All-Metal Baird Aromaticity. *Chem. Commun.* **2020**, *56*, 12522−12525.
(45) Alexandrova, A. N.; Boldyrev, A. I.; Zhai, H. J.; Wang, L. S. Electronic Structure, Isomerism, and Chemical Bonding in B_7^- and B_7. *J. Phys. Chem. A* **2004**, *108*, 3509−3517.
(46) Zhai, H. J.; Alexandrova, A. N.; Birch, K. A.; Boldyrev, A. I.; Wang, L. S. Hepta- and Octacoordinated Boron in Molecular Wheels of Eight- and Nine-Atom Boron Clusters: Observation and Confirmation. *Angew. Chem., Int. Ed.* **2003**, *42*, 6004−6008.
(47) Zhai, H. J.; Kiran, B.; Li, J.; Wang, L. S. Hydrocarbon Analogs of Boron Clusters: Planarity, Aromaticity, and Antiaromaticity. *Nat. Mater.* **2003**, *2*, 827−833.
(48) Alexandrova, A. N.; Boldyrev, A. I.; Zhai, H. J.; Wang, L. S. All-Boron Aromatic Clusters as Potential New Inorganic Ligands and Building Blocks in Chemistry. *Coord. Chem. Rev.* **2006**, *250*, 2811−2866.
(49) Zubarev, D. Y.; Boldyrev, A. I. Comprehensive Analysis of Chemical Bonding in Boron Clusters. *J. Comput. Chem.* **2007**, *28*, 251−268.
(50) Tai, T. B.; Grant, D. J.; Nguyen, M. T.; Dixon, D. A. Thermochemistry and Electronic Structure of Small Boron Clusters (B_n, n = 5−13) and Their Anions. *J. Phys. Chem. A* **2010**, *114*, 994−1007.
(51) Liao, Y.; Cruz, C. L.; Schleyer, P. v. R.; Chen, Z. Many M©B_n Boron Wheels Are Local, But Not Global Minima. *Phys. Chem. Chem. Phys.* **2012**, *14*, 14898−14904.
(52) Sergeeva, A. P.; Popov, I. A.; Piazza, Z. A.; Li, W. L.; Romanescu, C.; Wang, L. S.; Boldyrev, A. I. Understanding Boron through Size-Selected Clusters: Structure, Chemical Bonding, and Fluxionality. *Acc. Chem. Res.* **2014**, *47*, 1349−1358.
(53) Romanescu, C.; Galeev, T. R.; Li, W. L.; Boldyrev, A. I.; Wang, L. S. Transition-Metal-Centered Monocyclic Boron Wheel Clusters (M©B_n): A New Class of Aromatic Borometallic Compounds. *Acc. Chem. Res.* **2013**, *46*, 350−358.
(54) Wang, L. S. Photoelectron Spectroscopy of Size-Selected Boron Clusters: From Planar Structures to Borophenes and Borospherenes. *Int. Rev. Phys. Chem.* **2016**, *35*, 69−142.
(55) Boldyrev, A. I.; Wang, L. S. Beyond Organic Chemistry: Aromaticity in Atomic Clusters. *Phys. Chem. Chem. Phys.* **2016**, *18*, 11589−11605.
(56) Pham, H. T.; Lim, K. Z.; Havenith, R. W. A.; Nguyen, M. T. Aromatic Character of Planar Boron-Based Clusters Revisited by Ring Current Calculations. *Phys. Chem. Chem. Phys.* **2016**, *18*, 11919−11931.
(57) Li, W. L.; Chen, X.; Jian, T.; Chen, T. T.; Li, J.; Wang, L. S. From Planar Boron Clusters to Borophenes and Metalloborophenes. *Nat. Rev. Chem.* **2017**, *1*, 0071.
(58) Pan, S.; Barroso, J.; Jalife, S.; Heine, T.; Asmis, K. R.; Merino, G. Fluxional Boron Clusters: From Theory to Reality. *Acc. Chem. Res.* **2019**, *52*, 2732−2744.
(59) Duong, L. V.; Mai, D. T. T.; Pham-Ho, M. P.; Nguyen, M. T. A Theoretical Approach to the Role of Different Types of Electrons in Planar Elongated Boron Clusters. *Phys. Chem. Chem. Phys.* **2019**, *21*, 13030−13039.
(60) Jian, J.; Chen, X. N.; Li, S. D.; Boldyrev, A. I.; Li, J.; Wang, L. S. Probing the Structures and Bonding of Size-Selected Boron and Doped-Boron Clusters. *Chem. Soc. Rev.* **2019**, *48*, 3550−3591.
(61) Pyykko, P. Theoretical Chemsitry of Gold. III. *Chem. Soc. Rev.* **2008**, *37*, 1967−1997.
(62) Hakkinen, H. Atomic and Electronic Structure of Gold Clusters: Understanding Flakes, Cages and Superatoms from Simple Concepts. *Chem. Soc. Rev.* **2008**, *37*, 1847−1859.
(63) Schooss, D.; Weis, P.; Hampe, O.; Kappes, M. M. Determining the Size-Dependent Structure of Ligand-Free Gold-Cluster Ions. *Philos. Trans. R. Soc., A* **2010**, *368*, 1211−1243.
(64) Wang, L. M.; Wang, L. S. Probing the Electronic Properties and Structural Evolution of Anionic Gold Clusters in the Gas Phase. *Nanoscale* **2012**, *4*, 4038−4053.
(65) Woodham, A. P.; Fielicke, A. Gold Clusters in the Gas Phase. *Struct. Bonding (Berlin, Ger.)* **2013**, *161*, 243−278.
(66) Haruta, M. Size- and Support-Dependency in the Catalysis of Gold. *Catal. Today* **1997**, *36*, 153−166.
(67) Valden, M.; Lai, X.; Goodman, D. W. Onset of Catalytic Activity of Gold Clusters on Titania with the Appearance of Nonmetallic Properties. *Science.* **1998**, *281*, 1647−1650.
(68) Furche, F.; Ahlrichs, R.; Weis, P.; Jacob, C.; Gilb, S.; Bierweiler, T.; Kappes, M. M. The Structures of Small Gold Cluster Anions as Determined by a Combination of Ion Mobility Measurements and Density Functional Calculations. *J. Chem. Phys.* **2002**, *117*, 6982−6990.
(69) Johansson, M. P.; Lechtken, A.; Schooss, D.; Kappes, M. M.; Furche, F. *Phys. Rev. A: At., Mol., Opt. Phys.* **2008**, *77*, 053202.
(70) Huang, W.; Wang, L. S. Probing the 2D to 3D Structural Transition in Gold Cluster Anions Using Argon Tagging. *Phys. Rev. Lett.* **2009**, *102*, 153401.
(71) Pyykko, P. Relativistic Effects in Structural Chemistry. *Chem. Rev.* **1988**, *88*, 563−594.
(72) Pyykko, P. Theoretical Chemistry of Gold. *Angew. Chem., Int. Ed.* **2004**, *43*, 4412−4456.
(73) Hakkinen, H.; Moseler, M.; Landman, U. Bonding in Cu, Ag, and Au Clusters: Relativistic Effects, Trends, and Surprises. *Phys. Rev. Lett.* **2002**, *89*, 033401.
(74) Fernandez, E. M.; Soler, J. M.; Garzon, I. L.; Balbás, L. C. Trends in the structure and bonding of noble metal clusters. *Phys. Rev. B: Condens. Matter Mater. Phys.* **2004**, *70*, 165403.
(75) Xiong, X. G.; Xu, W. H.; Li, J.; Pyykko, P. Aspects of Bonding in Small Gold Clusters. *Int. J. Mass Spectrom.* **2013**, *354*−*355*, 15−18.
(76) Taylor, K. J.; Jin, C.; Conceicao, J.; Wang, L. S.; Cheshnovsky, O.; Johnson, B. R.; Nordlander, P. J.; Smalley, R. E. Vibrational Autodetachment Spectroscopy of Au_6^-: Image-Charge-Bound States of a Gold Ring. *J. Chem. Phys.* **1990**, *93*, 7515−7518.
(77) Hakkinen, H.; Landman, U. Gold Clusters (Au_N, N = 2−10) and Their Anions. *Phys. Rev. B: Condens. Matter Mater. Phys.* **2000**, *62*, R2287−R2290.
(78) Hakkinen, H.; Yoon, B.; Landman, U.; Li, X.; Zhai, H. J.; Wang, L. S. On the Electronic and Atomic Structures of Small Au_N^- (N = 4−14) Clusters: A Photoelectron Spectroscopy and Density-Functional Study. *J. Phys. Chem. A* **2003**, *107*, 6168−6175.
(79) Taylor, K. J.; Pettiette-Hall, C. L.; Cheshnovsky, O.; Smalley, R. E. Ultraviolet Photoelectron Spectra of Coinage Metal Clusters. *J. Chem. Phys.* **1992**, *96*, 3319−3329.
(80) Tanaka, H.; Neukermans, S.; Janssens, E.; Silverans, R. E.; Lievens, P. T Aromaticity of the Bimetallic Au_5Zn^+ Cluster. *J. Am. Chem. Soc.* **2003**, *125*, 2862−2863.
(81) Lin, L.; Holtzl, T.; Gruene, P.; Claes, P.; Meijer, G.; Fielicke, A.; Lievens, P.; Nguyen, M. T. Fluxionality and σ-Aromaticity in Small Yttrium-Doped Gold Clusters. *ChemPhysChem* **2008**, *9*, 2471−2474.
(82) Huang, W.; Wang, L. S. Au_{10}^-: Isomerism and Structure-Dependent O_2 Reactivity. *Phys. Chem. Chem. Phys.* **2009**, *11*, 2663−2667.
(83) Bulusu, S.; Li, X.; Wang, L. S.; Zeng, X. C. Evidence of Hollow Golden Cages. *Proc. Natl. Acad. Sci. U. S. A.* **2006**, *103*, 8326−8330.
(84) Salisbury, B. E.; Wallace, W. T.; Whetten, R. L. Low-Temperature Activation of Molecular Oxygen by Gold Clusters: A Stoichiometric Process Correlated to Electron Affinity. *Chem. Phys.* **2000**, *262*, 131−141.
(85) Wang, L. M.; Bulusu, S.; Zhai, H. J.; Zeng, X. C.; Wang, L. S. Doping Golden Buckyballs: Cu@Au_{16}^- and Cu@Au_{17}^- Cluster Anions. *Angew. Chem., Int. Ed.* **2007**, *46*, 2915−2918.
(86) Tanaka, H.; Neukermans, S.; Janssens, E.; Silverans, R.; Lievens, P. Density Functional Study on Structure and Stability of

https://doi.org/10.1021/acs.jpca.1c02954
J. Phys. Chem. A 2021, 125, 4606−4613

Bimetallic Au_NZn (N < 6) Clusters and Their Cations. *J. Chem. Phys.* **2003**, *119*, 7115−7123.
(87) Janssens, E.; Tanaka, H.; Neukermans, S.; Silverans, R. E.; Lievens, P. Two-dimensional Magic Numbers in Mass Abudances of Photofragmented Bimetallic Clusters. *New J. Phys.* **2003**, *5*, 46.
(88) Koyasu, K.; Naono, Y.; Akutsu, M.; Mitsui, M.; Nakajima, A. Photoelectron Spectroscopy of Binary Au Cluster Anions with a Doped Metal Atom: Au_nM^- (n = 2−7), M = Pd, Ni, Zn, Cu, and Mg. *Chem. Phys. Lett.* **2006**, *422*, 62−66.
(89) Wang, L. M.; Pal, R.; Huang, W.; Zeng, X. C.; Wang, L. S. Observation of Earlier Two to Three Dimensional Structural Transition in Gold Cluster Anions by Isoelectronic Substitution: MAu_n^-(n = 8−11; M = Ag, Cu). *J. Chem. Phys.* **2010**, *132*, 114306.
(90) Lin, L.; Claes, P.; Gruene, P.; Meijer, G.; Fielicke, A.; Nguyen, M. T.; Lievens, P. Far-Infrared Spectra of Yttrium-Doped Gold Clusters Au_nY (n = 1−9). *ChemPhysChem* **2010**, *11*, 1932−1943.
(91) Wang, H. Q.; Kuang, X. Y.; Li, H. F. Structural, Electronic, and Magnetic Properties of Gold Cluster Anions Doped with Zinc: Au_nZn^- (n = 2−10). *J. Phys. Chem. A* **2009**, *113*, 14022−14028.
(92) Wang, L. S.; Cheng, H. S.; Fan, J. Photoelectron Spectroscopy of Size-Selected Transition Metal Clusters: Fe_n^-, n = 3−24. *J. Chem. Phys.* **1995**, *102*, 9480−9493.
(93) Zhai, H.; Ha, M.-A.; Alexandrova, A. N. AFFCK: Adaptive Force-Field-Assisted Ab Initio Coalescence Kick Method for Global Minimum Search. *J. Chem. Theory Comput.* **2015**, *11*, 2385−2393.
(94) Adamo, C.; Barone, V. Toward Reliable Density Functional Methods without Adjustable Parameters: The PBE0Model. *J. Chem. Phys.* **1999**, *110*, 6158−6170.
(95) Frisch, M. J.; Trucks, G. W.; Schlegel, H. B.; Scuseria, G. E.; Robb, M. a.; Cheeseman, J. R.; Scalmani, G.; Barone, V.; Petersson, G. a.; Nakatsuji, H. et al. G16_C01; *Gaussian 16*, Revision C.01, Gaussian, Inc.: Wallingford, CT, 2016.
(96) Neese, F. The ORCA Program System. *Wiley Interdiscip. Rev.: Comput. Mol. Sci.* **2012**, *2*, 73−78.
(97) Zhao, Y.; Chen, X.; Li, J. TGMin: A Global-Minimum Structure Search Program Based on a Constrained Basin-Hopping Algorithm. *Nano Res.* **2017**, *10*, 3407−3420.
(98) te Velde, G.; Bickelhaupt, F. M.; Baerends, E. J.; Fonseca Guerra, C.; van Gisbergen, S. J. A.; Snijders, J. G.; Ziegler, T. Chemistry with ADF. *J. Comput. Chem.* **2001**, *22*, 931−967.
(99) Fonseca Guerra, C.; Snijders, J. G.; Te Velde, G.; Baerends, E. J. Towards an Order-N DFT Method. *Theor. Chem. Acc.* **1998**, *99*, 391−403.
(100) Lenthe, E. v.; Baerends, E. J.; Snijders, J. G. Relativistic Regular Two-component Hamiltonians. *J. Chem. Phys.* **1993**, *99*, 4597−4610.
(101) Dau, P. D.; Su, J.; Liu, H. T.; Liu, J. B.; Huang, D. L.; Li, J.; Wang, L. S. Observation and Investigation of the Uranyl Tetrafluoride Dianion ($UO_2F_4^{2-}$) and Its Solvation Complexes with Water and Acetonitrile. *Chem. Sci.* **2012**, *3*, 1137−1146.
(102) Dau, P. D.; Su, J.; Liu, H. T.; Huang, D. L.; Li, J.; Wang, L. S. Photoelectron Spectroscopy and the Electronic Structure of the Uranyl Tetrachloride Dianion: $UO_2Cl_4^{2-}$. *J. Chem. Phys.* **2012**, *137*, 064315.
(103) Stowasser, R.; Hoffmann, R. What Do the Kohn-Sham Orbitals and Eigenvalues Mean? *J. Am. Chem. Soc.* **1999**, *121*, 3414−3420.
(104) Chong, D. P.; Gritsenko, O. V.; Baerends, E. J. Interpretation of the Kohn-Sham Orbital Energies as Approximate Vertical Ionization Potentials. *J. Chem. Phys.* **2002**, *116*, 1760−1772.
(105) Zubarev, D. Y.; Boldyrev, A. I. Developing Paradigms of Chemical Bonding: Adaptive Natural Density Partitioning. *Phys. Chem. Chem. Phys.* **2008**, *10*, 5207−5217.
(106) Zubarev, D. Y.; Boldyrev, A. I. Revealing Intuitively Assessable Chemical Bonding Patterns in Organic Aromatic Molecules via Adaptive Natural Density Partitioning. *J. Org. Chem.* **2008**, *73*, 9251−9258.
(107) Tkachenko, N. V.; Boldyrev, A. I. Chemical Bonding Analysis of Excited States Using the Adaptive Natural Density Partitioning Method. *Phys. Chem. Chem. Phys.* **2019**, *21*, 9590−9596.
(108) Zhai, H. J.; Kiran, B.; Dai, B.; Li, J.; Wang, L. S. Unique CO Chemisorption Properties of Gold Hexamer: $Au_6(CO)_n^-$ (n = 0−3). *J. Am. Chem. Soc.* **2005**, *127*, 12098−12106.
(109) Baird, N. C. Quantum Organic Photochemistry. II. Resonance and Aromaticity in the Lowest $^3\gg^*$ State of Cyclic Hydrocarbons. *J. Am. Chem. Soc.* **1972**, *94*, 4941−4948.

https://doi.org/10.1021/acs.jpca.1c02954
J. Phys. Chem. A 2021, 125, 4606−4613